Article

Cell Reports

# Taxane-Platin-Resistant Lung Cancers Co-develop Hypersensitivity to JumonjiC Demethylase Inhibitors

## Graphical Abstract

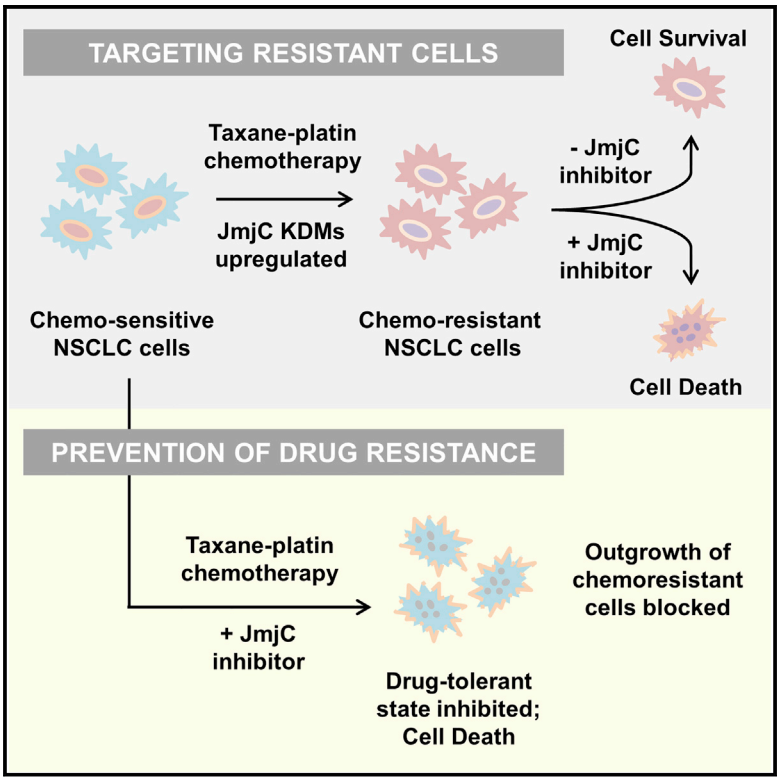


## Authors

Maithili P. Dalvi, Lei Wang, Rui Zhong, ..., Ignacio I. Wistuba, John D. Minna, Elisabeth D. Martinez

## Correspondence

elisabeth.martinez@utsouthwestern.edu

## In Brief

Taxane-platin chemotherapy for non-small cell lung cancer (NSCLC) is beneficial, yet most tumors become drug resistant. Dalvi et al. find upregulation of JumonjiC demethylases in clinical NSCLC samples and preclinical models of resistance. Resistant cells and tumors show hypersensitivity to JumonjiC inhibitors, suggesting a therapeutic opportunity for targeting taxane-platin resistance.

## Highlights

- Taxane-platin-resistance signature correlates with cancer relapse in NSCLC patients
- Resistant cells upregulate JmjC demethylases and alter histone methylation levels
- Taxane-platin-resistant cells and tumors develop hypersensitivity to JmjC inhibitors
- JmjC inhibition prevents emergence of taxane-platin-tolerant colonies

## Accession Numbers

GSE77209
GSE81689

Dalvi et al., 2017, Cell Reports *19*, 1669–1684
May 23, 2017 
http://dx.doi.org/10.1016/j.celrep.2017.04.077

Cell Reports
Article



# Taxane-Platin-Resistant Lung Cancers Co-develop Hypersensitivity to JumonjiC Demethylase Inhibitors

Maithili P. Dalvi,[1,2] Lei Wang,[1,4] Rui Zhong,[3] Rahul K. Kollipara,[5] Hyunsil Park,[1] Juan Bayo,[1,4] Paul Yenerall,[1,2,5] Yunyun Zhou,[3] Brenda C. Timmons,[1,2] Jaime Rodriguez-Canales,[7] Carmen Behrens,[8] Barbara Mino,[7] Pamela Villalobos,[7] Edwin R. Parra,[7] Milind Suraokar,[7] Apar Pataer,[9] Stephen G. Swisher,[9] Neda Kalhor,[10] Natarajan V. Bhanu,[11] Benjamin A. Garcia,[11] John V. Heymach,[8] Kevin Coombes,[12] Yang Xie,[3] Luc Girard,[1,4] Adi F. Gazdar,[1,2] Ralf Kittler,[2,4,5] Ignacio I. Wistuba,[7,8] John D. Minna,[1,2,4,6] and Elisabeth D. Martinez[1,2,4,13,*]
[1]Hamon Center for Therapeutic Oncology Research
[2]Simmons Comprehensive Cancer Center
[3]Department of Clinical Science
[4]Department of Pharmacology
[5]Eugene McDermott Center for Human Growth and Development
[6]Department of Internal Medicine
The University of Texas Southwestern Medical Center, Dallas, TX 75390, USA
[7]Department of Translational Molecular Pathology
[8]Department of Thoracic/Head and Neck Medical Oncology
[9]Department of Thoracic and Cardiovascular Surgery
[10]Department of Pathology
The University of Texas MD Anderson Cancer Center, Houston, TX 77030, USA
[11]Epigenetics Program, Department of Biochemistry and Biophysics, Perelman School of Medicine, University of Pennsylvania, Philadelphia, PA 19104, USA
[12]Department of Biomedical Informatics, The Ohio State University College of Medicine, Columbus, OH 43210, USA
[13]Lead Contact
*Correspondence: elisabeth.martinez@utsouthwestern.edu
http://dx.doi.org/10.1016/j.celrep.2017.04.077

## SUMMARY

**Although non-small cell lung cancer (NSCLC) patients benefit from standard taxane-platin chemotherapy, many relapse, developing drug resistance. We established preclinical taxane-platin-chemoresistance models and identified a 35-gene resistance signature, which was associated with poor recurrence-free survival in neoadjuvant-treated NSCLC patients and included upregulation of the JumonjiC lysine demethylase *KDM3B*. In fact, multi-drug-resistant cells progressively increased the expression of many JumonjiC demethylases, had altered histone methylation, and, importantly, showed hypersensitivity to JumonjiC inhibitors in vitro and in vivo. Increasing taxane-platin resistance in progressive cell line series was accompanied by progressive sensitization to JIB-04 and GSK-J4. These JumonjiC inhibitors partly reversed deregulated transcriptional programs, prevented the emergence of drug-tolerant colonies from chemo-naive cells, and synergized with standard chemotherapy in vitro and in vivo. Our findings reveal JumonjiC inhibitors as promising therapies for targeting taxane-platin-chemoresistant NSCLCs.**

## INTRODUCTION

Lung cancer is the leading cause of cancer-related deaths in the United States (American Cancer Society, 2015; Howlader et al., 1975–2012). Non-small cell lung cancer (NSCLC) accounts for 85% of all lung cancer cases, more than 50% of which are already at an advanced stage at the time of diagnosis. Platinum-based doublet chemotherapy is the standard of care for advanced NSCLCs and is given in combination with third-generation cytotoxic agents such as paclitaxel (Scagliotti et al., 2008; Schiller et al., 2002). Early-stage patients also receive platin-taxane chemotherapy to shrink tumors prior to resection (neoadjuvant therapy). Cancer relapse after chemotherapy poses a major obstacle for lung cancer cure, and multiple studies have reported recurrence/drug resistance in ~70% of treated patients (Martin et al., 2002; Massarelli et al., 2003; d'Amato et al., 2007). Thus, despite current advances in targeted therapy for lung cancer, there is a large unmet clinical need to identify effective therapies for chemotherapy-resistant NSCLCs.

The most commonly implicated mechanism for acquisition of resistance to taxanes involves increased expression of drug efflux transporters such as MDR1, resulting in cross-resistance to other chemotherapies (Gottesman et al., 2002). Clinical trials using MDR inhibitors have been unsuccessful because of associated toxicity to normal tissues or lack of response due to collateral mechanisms of resistance (Bradshaw and Arceci, 1998; Szakács et al., 2006). Epigenetic drivers of tumor drug tolerance

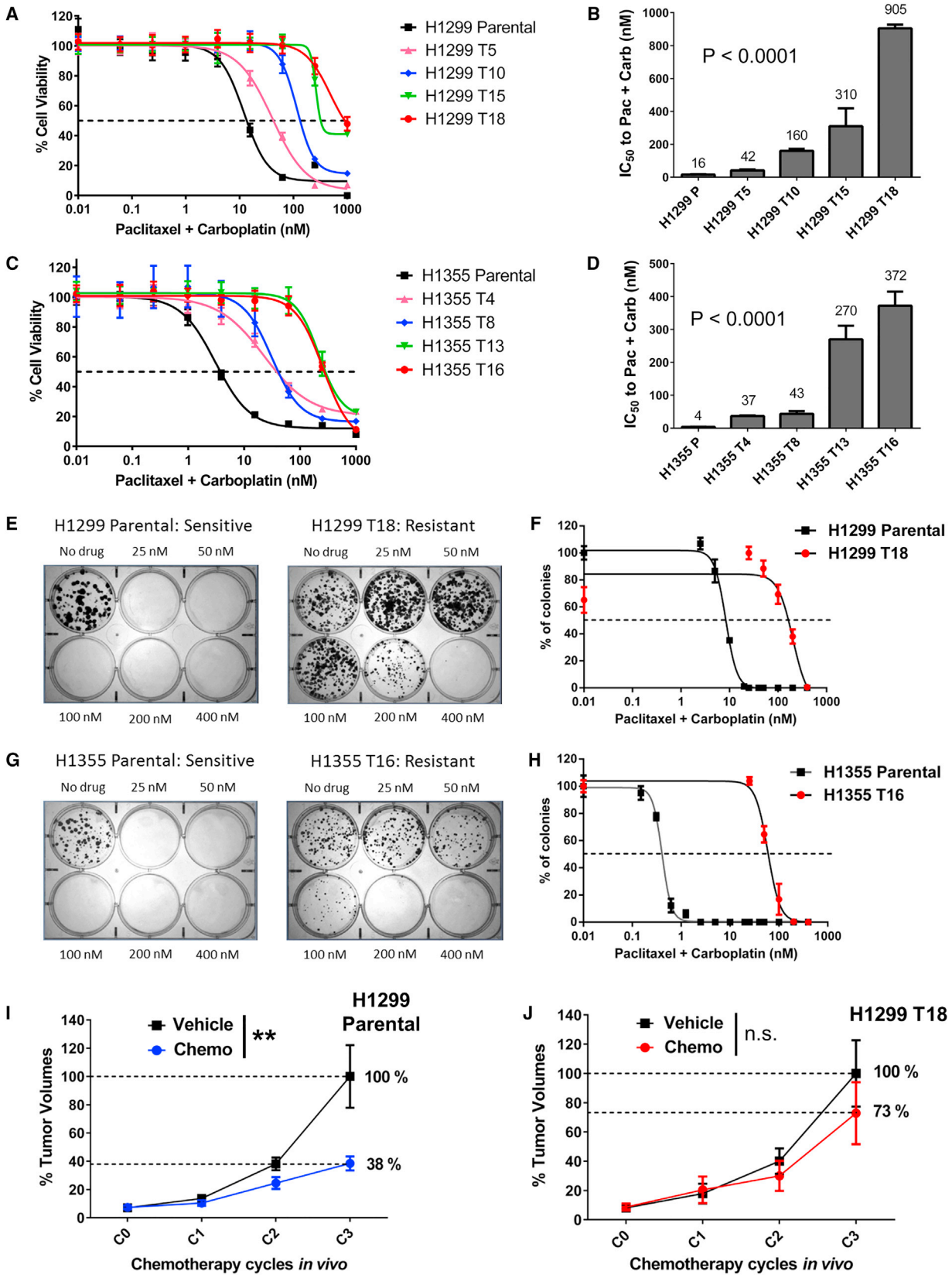


(legend on next page)

have recently gained attention owing to their ability to dynamically alter transcriptional programs. Cell subpopulations surviving epidermal growth factor receptor (EGFR) tyrosine kinase inhibitor or $BRAF^{V600E}$ inhibitor overexpress the histone lysine demethylase KDM5A (Sharma et al., 2010) or KDM5B (Roesch et al., 2013), respectively, and KDM5 inhibitors have recently shown therapeutic potential (Vinogradova et al., 2016). T cell acute lymphoblastic leukemia cells persisting gamma-secretase inhibitors showed increased expression of BRD4 and sensitivity to the small-molecule inhibitor JQ1 (Knoechel et al., 2014). These studies suggest a role of epigenetic drivers in the acquisition of the drug-tolerant state. This state might not only provide a transition phase for surviving drug stress but also lead the way to establishing permanent resistance mechanisms.

To study the progression of NSCLC resistance to standard taxane-platin combination therapy, we developed isogenic resistant cell line variants through long-term drug treatment using cycles of drug on/drug off therapy to mimic clinical regimens. We then used these models to search for clinically relevant targets for drug-resistant lung cancers by integrating genome-wide mRNA expression profiles of resistant cell line variants and the corresponding xenografts and by evaluating the preclinical resistance signature for its association with recurrence-free survival outcome in neoadjuvant-chemotherapy-treated NSCLC patients. Intriguingly, our studies uncovered epigenetic alterations in chemoresistant cells encompassing several members of the JumonjiC (JmjC) histone demethylase family. We asked whether these epigenetic mechanisms conferred a survival advantage that could be exploited therapeutically to abrogate NSCLC cells that develop resistance to taxane-platin chemotherapy.

## RESULTS

### Long-Term Paclitaxel-Carboplatin-Treated NSCLC Cell Lines Develop Progressive Increases in Chemoresistance

To establish in vitro models of lung cancer chemoresistance, we treated NSCLC cell lines with paclitaxel-carboplatin standard chemotherapy, which was given in the clinically relevant 2:3 w/w ratio. Our ongoing tests of >100 NSCLC lines identified H1299 and H1355 among a group of NSCLC cell lines that had 100- to 500-fold lower half inhibitory concentration ($IC_{50}$) values than the most resistant NSCLC lines and were thus selected as "parental" cells to develop drug-resistant variants. Clinical annotations and driver oncogenotypes for these cell lines are listed in Table S1. H1299 and H1355 cells were treated long-term (>6 months) with increasing doses of paclitaxel-carboplatin doublet, given in cycles of drug on (4 days) and drug off (1–2 weeks). Cells were characterized for their drug-response phenotypes after different treatment cycles, with T[n] denoting cell line variant developed after "n" cycles of doublet therapy. We thus developed H1299 variant series consisting of T5, T10, T15, and T18 and H1355 isogenic cell line series with T4, T8, T13, and T16 resistant variants. These variants showed progressive increase in resistance to paclitaxel-carboplatin with increasing treatment cycles (Figures 1A and 1C), reaching >50-fold increases in $IC_{50}$ in H1299 T18 and H1355 T16 (Figures 1B and 1D). Drug resistance persisted in limiting dilution clonogenic assays with continuous exposure to paclitaxel-carboplatin for 2–3 weeks (Figures 1E–1H).

### Resistant Cell Line Variants Show Decreased Response to Taxane-Platin Chemotherapy In Vivo and Cross-Resistance to Multiple Drugs In Vitro

To validate the taxane-platin resistance phenotype in vivo, we grew subcutaneous xenografts of H1299 parental and H1299 T18 cells and treated tumor-bearing mice with three cycles of docetaxel-cisplatin doublet chemotherapy. While H1299 parental xenografts showed a dramatic reduction in tumor burden compared to the vehicle-treated group (Figure 1I; **p = 0.002), H1299 T18 tumors showed a non-significant response, confirming resistance (Figure 1J). This also confirmed cross-resistance to docetaxel-cisplatin standard therapy.

Consistent with previously published reports that suggested the involvement of MDR1 in taxane resistance (Lemontt et al., 1988; Roninson et al., 1986), we detected increased mRNA and protein expression of MDR1 in both H1299- and H1355-resistant variants (Figures S1A–S1D), decreased drug accumulation (Figure S1E), and partial re-sensitization to the doublet upon genetic/pharmacological inhibition (Figures S1F–S1H). To characterize the multi-drug-resistance phenotype, we tested several standard and targeted agents (Figure S2A). Resistant variants were found to be cross-resistant to docetaxel, doxorubicin, vinorelbine, and depsipeptide, which are known MDR1 substrates (Figure S2B). Cells remained sensitive to carboplatin as single agent, consistent with the low dose used and its established mechanism of action (Busschots et al., 2015). Extended

**Figure 1. Long-Term-Treated NSCLC Cell Lines Develop Progressively Increasing Resistance to Paclitaxel-Carboplatin Chemotherapy**

(A and C) Dose-response curves for NCI-H1299 (A) and NCI-H1355 (C) cells after long-term treatment with drug on/drug off cycles of paclitaxel-carboplatin. P, parental cell line; T[n], resistant variant generated after "n" cycles of doublet chemotherapy. Values on the x axis indicate paclitaxel concentration (nM) in the drug combination (see Experimental Procedures for dosing details). Each data point represents mean ± SD of eight replicates.

(B and D) $IC_{50}$ plots for H1299 (B) and H1355 (D) resistant cell line variants. $IC_{50}$ values represent paclitaxel concentration (in nM) in the 2:3 w/w drug combination. Data represent $IC_{50}$ mean ± SD of four or more replicate assays. p values are from post-test for linear trend following one-way ANOVA.

(E and G) Resistance was validated in liquid colony formation assays. Representative plate images for H1299 (E) and H1355 (G) cells are shown. Drug values indicate concentration of paclitaxel (in nM) in the 2:3 w/w doublet.

(F and H) Dose-response curves for H1299 (F) and H1355 (H) were generated by counting stained colonies from colony-formation assays. For parental cell lines, additional plates were treated with lower doses starting from 40 nM highest dose for two-fold serial dilutions. Error bars represent mean ± SEM.

(I and J) H1299 parental (I) and H1299 T18 (J) tumor-bearing mice were randomized (n = 8 per group) to receive vehicle or docetaxel + cisplatin once a week for 3 weeks. Tumor volumes were measured after each treatment cycle (C1, C2, and C3). Error bars represent mean ± SEM. Groups were compared using two-way ANOVA followed by Sidak's multiple comparison tests. H1299 parental xenografts, two-way ANOVA: **p = 0.002, Sidak's test at C3: ****p < 0.0001; H1299 T18 xenografts, two-way ANOVA: p value not significant (n.s.).

See Table S1 and related Figures S1–S3.

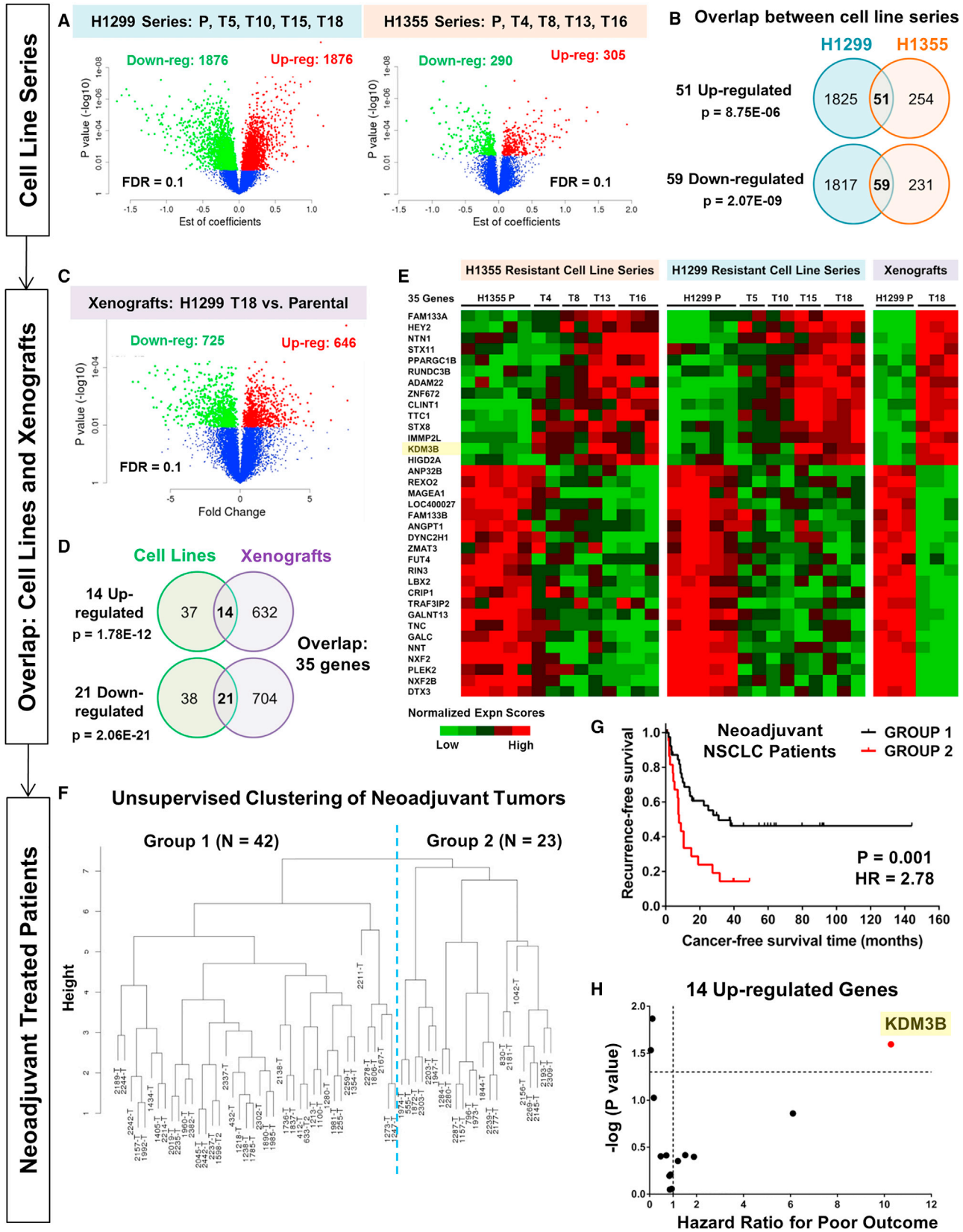


(legend on next page)

drug-free culturing for >4 months resulted in partial reversal of paclitaxel-carboplatin resistance (Figures S2C–S2F), suggesting transient mechanisms in addition to stable changes. When we expanded our panel of drug-resistant models to H1693 and HCC4017 cell lines, we found that both developed taxane-platin resistance upon long-term exposure (Figures S3A–S3D), but HCC4017 T5 did not show increased MDR1 (Figures S3E–S3H). These findings led us to investigate other molecular changes in taxane-platin resistance.

## Gene Expression Profiles of Preclinical Models Yield a Resistance-Associated Gene Signature

To investigate the molecular changes accompanying the development of NSCLC resistance to chemotherapy, we performed genome-wide mRNA expression profiling of the entire progressively resistant, isogenic H1299 and H1355 cell line series. We fitted a linear regression model on microarray data to systematically identify genes that showed a progressive increase or decrease in expression consistent with increasing drug resistance represented by the log-transformed $IC_{50}$ values across the entire series of progressed lines. We identified 3,752 differentially expressed genes in the H1299-resistant series and 595 genes in the H1355-resistant series at a false discovery rate of 0.1 (Figure 2A). We then performed stringent filtering of expression data to only select for genes that exhibited overlap between the two progressively resistant NSCLC cell line models. We further required these changes to occur in vivo in H1299 xenografts. 51 upregulated and 59 downregulated genes overlapped between the H1299- and H1355-resistant cell line series (Figure 2B), while intersection with xenograft tumor profiles (H1299 T18 versus H1299 parental xenografts; Figure 2C) identified 14 upregulated and 21 downregulated genes whose expression differences were sustained in vivo (Figure 2D). These 35 genes (Figure 2E) formed our preclinical resistance signature.

## Evaluation of Preclinical Resistance Signature in Neoadjuvant-Treated NSCLC Patient Tumors Identified KDM3B as an Important Correlate of Poor Recurrence-Free Outcome and a Druggable Resistance Target

To identify clinically relevant drug-resistance targets, we tested our 35-gene resistance signature on a cohort of 65 NSCLC patients (annotated in Table S2) who had received platin-based neoadjuvant chemotherapy, with taxane-platin doublet administered prior to surgical resection. Resected tumor samples were profiled by microarrays. Based on the 35-gene preclinical signature, unsupervised hierarchical clustering separated the chemotherapy-treated patient tumors into two major groups (Figure 2F). Kaplan-Meier survival analysis revealed significant differences in recurrence-free survival (Figure 2G). Group 2 exhibited significantly worse cancer recurrence-free prognosis than Group 1 patients (hazard ratio = 2.78, p = 0.001, adjusted for clinical covariates in Table S3).

We further evaluated the individual contribution of the 35 genes in the signature using Cox multivariate regression (Table S4) and focused on upregulated genes as potential therapeutic targets. Among the 14 genes that were commonly upregulated in preclinical resistance models, the gene that showed the largest hazard risk for poor recurrence-free outcome in neoadjuvant-treated NSCLC patients was the JmjC lysine demethylase KDM3B (hazard ratio = 10.28, p = 0.025; Figure 2H), a druggable enzyme. Notably, two of the downregulated genes in our 35-gene signature, MAGEA1 and ANGPT1, are known to be suppressed by KDM3B (GEO: GSE30294) (Kim et al., 2012). We thus decided to explore KDM3B given that it represents an actionable enzyme target.

## Neoadjuvant-Treated NSCLC Tumors Show Increased KDM Expression

KDM3B protein levels were evaluated in the same cohort of neoadjuvant-chemotherapy-treated NSCLC tumors by immunohistochemistry (IHC) of specimens available in a tissue microarray. Group 2 patients (who had poor recurrence-free survival) showed higher overall KDM3B IHC scores than Group 1 patients (Figure 3A). We then evaluated the mRNA expression of other members of the KDM enzyme family in the NSCLC patients (66 neoadjuvant treated and 209 chemo-naive; annotated in Table S2). NSCLC patient tumor cells surviving standard neoadjuvant chemotherapy expressed higher overall *KDM3A* and *KDM4A* mRNA levels than chemo-naive tumors (Figure 3B; p value adjusted for clinical variables by multivariate analysis shown in Table S5).

**Figure 2. Gene Signature from Chemoresistant Models Clusters Neoadjuvant-Treated NSCLC Patients Based on Relapse-free Outcome and Identifies *KDM3B* as a Significant Contributor to Poor Recurrence-free Survival**

(A) Linear regression model was fitted on microarray data to identify genes that were progressively up-/ downregulated with increasing drug resistance. Parental cell lines (P) and four resistant variants per model were analyzed. Differentially expressed genes are represented in the volcano plots (red, upregulated; green, downregulated). FDR = 0.1.

(B) Common up- and downregulated genes across the two resistant cell line series are shown. p values are from hypergeometric tests.

(C) Differential gene expression analysis on xenograft microarray data (H1299 T18 resistant versus H1299 parental) using Student's t test. FDR = 0.1.

(D) Gene lists obtained from cell line and xenograft microarray analyses were overlapped to identify common genes (14 upregulated, 21 downregulated). p values are from hypergeometric tests.

(E) Heatmap representation of the expression pattern of 35-gene resistance signature in resistant cell lines and xenografts.

(F) Using mRNA expression of 35 genes, unsupervised hierarchical clustering of neoadjuvant-treated NSCLC patients (n = 65, mainly taxane-platin treated) was found to separate the patients into two major groups.

(G) Kaplan-Meier survival analysis of the two groups of neoadjuvant-treated NSCLC patients revealed significant differences in cancer recurrence-free survival (p = 0.001; hazard ratio = 2.78; 95% confidence interval [CI], 1.46–5.29). Survival p value was adjusted for clinical covariates (Cox multivariate regression; Table S3).

(H) Cox multivariate regression identified individual contributions of the 35 genes to poor recurrence-free survival (Table S4). The x axis depicts hazard ratios (i.e., exp [regression coefficient]), and the y axis represents −log (p values) for the 14 upregulated genes. *KDM3B* showed the largest hazard risk for poor recurrence-free patient survival (hazard ratio = 10.28, p = 0.025).

See Tables S2–S4.

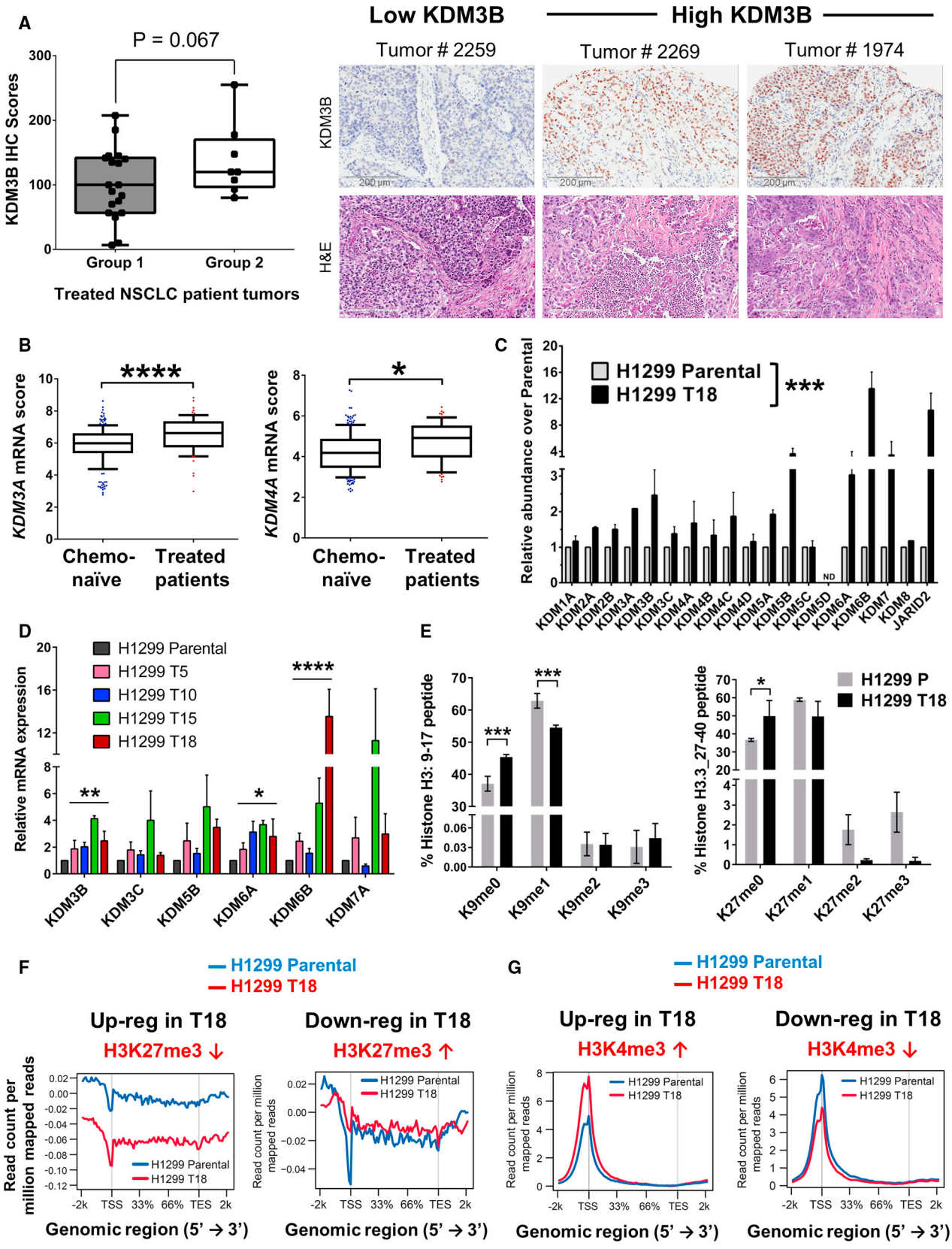


(legend on next page)

## Chemoresistant Cells Show Increased Expression of JmjC Histone Lysine Demethylases and Altered Histone Methylation Levels

Although *KDM3B* was the only histone demethylase that made it into the 35-gene resistance signature because it was progressively upregulated throughout the resistant series, was common to both H1299 and H1355 cell line models, and showed increased expression in vivo, several other JmjC family members were also overexpressed in resistant models. For example, *KDM5A*, *JMJD4*, and *JMJD8* were among the other upregulated genes in the H1299-resistant cell line series (false discovery rate [FDR] = 0.1, $p < 0.05$). In-vivo-grown H1299 T18 tumors exhibited increased expression of *KDM3A*, *KDM4B*, *KDM5A*, *KDM5B*, *KDM6B*, *KDM7A*, *JARID2*, *JMJD4*, and *JMJD6* (Figure S4A).

We therefore profiled the JmjC KDM gene family in chemoresistant versus parental cells by qRT-PCR and found general upregulation of JmjC KDMs, including *KDM3B* (Figures 3C and S4B). We also noted strong upregulation of the H3K27 demethylases *KDM6A*, *KDM6B*, and *KDM7A,* and modest upregulation of the H3K4 demethylases *KDM5A* and *KDM5B* in H1299 T18 cells (Figure 3C). We then queried the entire progressively resistant H1299 series and found a consistent increase in KDM mRNA expression with increasing resistance to paclitaxel-carboplatin chemotherapy (Figure 3D).

To investigate the functional effects of JmjC KDM upregulation in resistant cells, we performed mass spectrometry for global histone post-translational modifications in histone extracts from H1299 T18 and H1299 parental cells. Consistent with the upregulation of the H3K9me1 demethylase KDM3B, we detected a global decrease in H3K9me1 and a subsequent increase in H3K9me0 in H1299 T18 versus parental cells (Figure 3E, left). We also found decreased K9me1 in K14 acetylated H3 and a corresponding increase in K9/K14 unmodified (me0, ac0) levels in both H1299 T18 and H1355 T16 cell lines (Figure S4C). In agreement with strong upregulation of the histone3 K27me3/me2 demethylase KDM6B in H1299 T18 cells, we observed decreased K27me3 and K27me2 global levels and a corresponding increase in K27me0 (Figure 3E, right) on H3.3, a histone3 variant deposited specifically in actively transcribed regions (Szenker et al., 2011).

To gain insights into the effect of increased H3K27 and H3K4 demethylases on the transcriptional output of chemoresistant cells, we performed chromatin immunoprecipitation sequencing (ChIP-seq) for H3K27me3 and H3K4me3 marks in H1299 parental and H1299 T18 cells. First, correlating with increased expression of H3K27me3 demethylases, we observed that H1299-T18-resistant cells showed marked decrease in the "average" distribution of H3K27me3 across all transcribed regions of the genome (Figure S4D). There was however no decrease in average H3K4me3 distribution across all genes (Figure S4E). To specify the transcribed regions that exhibited changes in H3K27me3 and identify altered H3K4me3 enrichment, we used RNA sequencing (RNA-seq) to classify differentially upregulated and downregulated genes in H1299 T18 versus H1299 parental cells (fragments per kilobase of transcript per million mapped reads [FPKM] $\geq 1$; FDR q = 0.05) and then evaluated their histone marks. We found that the upregulated genes in H1299 T18 showed an overall decrease in the repressive H3K27me3 signal throughout transcription start sites (TSSs) and gene bodies (Figure 3F, left), whereas downregulated genes selectively showed increased H3K27me3 at the TSS (Figure 3F, right). Likewise, ChIP-seq for H3K4me3 revealed an increase in H3K4me3 at the TSS of upregulated genes (Figure 3G, left), while downregulated genes exhibited reduced H3K4me3 at the TSS (Figure 3G, right). We thus detected functional changes in the H3K4/H3K27 methylation landscape of resistant versus parental cells that corresponded with transcriptional activation or repression of differentially expressed genes.

## Chemoresistant Cells Are Hypersensitized to JmjC Demethylase Inhibitors

To test the survival dependency of chemoresistant cells on JmjC KDMs, we first employed a pan-selective JmjC demethylase inhibitor, JIB-04 (Wang et al., 2013). H1299 T18 cells were several-fold hypersensitized to JIB-04 E isomer compared to parental cells (Figure 4A), while the inactive Z isomer had no effect. We then tested the KDM5/KDM6 subfamily inhibitor GSK-J4 (Kruidenier et al., 2012). Again, H1299 T18 showed higher sensitivity

**Figure 3. Neoadjuvant-Treated NSCLC Patient Tumors and Chemoresistant Cell Lines Exhibit Elevated Expression of JmjC Histone Demethylases and Altered Histone Methylation**

(A) Group 2 of neoadjuvant-treated patients (poor recurrence-free survival) showed higher KDM3B IHC scores than Group 1 patients. Representative images of KDM3B IHC and corresponding tumor H&E staining are shown. Scale bar, 200 μm.

(B) Chemotherapy-treated patient tumors showed higher mRNA expression scores of *KDM3A* and *KDM4A* than chemo-naive tumors. The y axis depicts $\log_2$ normalized expression scores. The line indicates median value and whiskers the 10$^{th}$ and 90$^{th}$ percentiles. p values are adjusted after multivariate analysis of clinical variables (*$p < 0.05$, ****$p < 0.0001$).

(C) Paclitaxel-carboplatin-resistant H1299 T18 cell line showed increased mRNA expression of several JmjC KDMs compared to H1299 parental, by qRT-PCR. Error bars represent mean ± SEM. p values are from two-way ANOVA (***$p < 0.001$).

(D) Isogenic H1299 resistant cells showed progressive increases in JmjC KDM expression. Error bars represent mean ± SEM. p values are from one-way ANOVA post-test for linear trend (*$p < 0.05$, **$p < 0.01$, ****$p < 0.0001$).

(E) Global changes in histone lysine methylation were measured by mass spectrometry. The y axis denotes the percentage of the stated histone peptides (left, H3: 9–17; right, H3.3: 27–40) that showed K9 or K27 methylation, respectively. Left panel error bars represent mean ± SEM (n = 3). Right panel error bars represent mean ± SEM (n = 2). p values are from Fisher's LSD test post two-way ANOVA, *$p < 0.1$, ***$p < 0.001$.

(F) H3K27me3 ChIP-seq enrichment plots for up- and downregulated genes identified by RNA-Seq (FDR 0.05) in H1299 T18 versus H1299 parental cells. x axis represents the genomic regions from 5′ to 3′ and the y axis represents read depth.

(G) H3K4me3 average distribution plots for differentially expressed genes in H1299 T18 versus H1299 Parental cells (left panel upregulated, right panel downregulated genes). TSS, transcription start site; TES, transcription end site.

See also Table S5 and Figure S4.

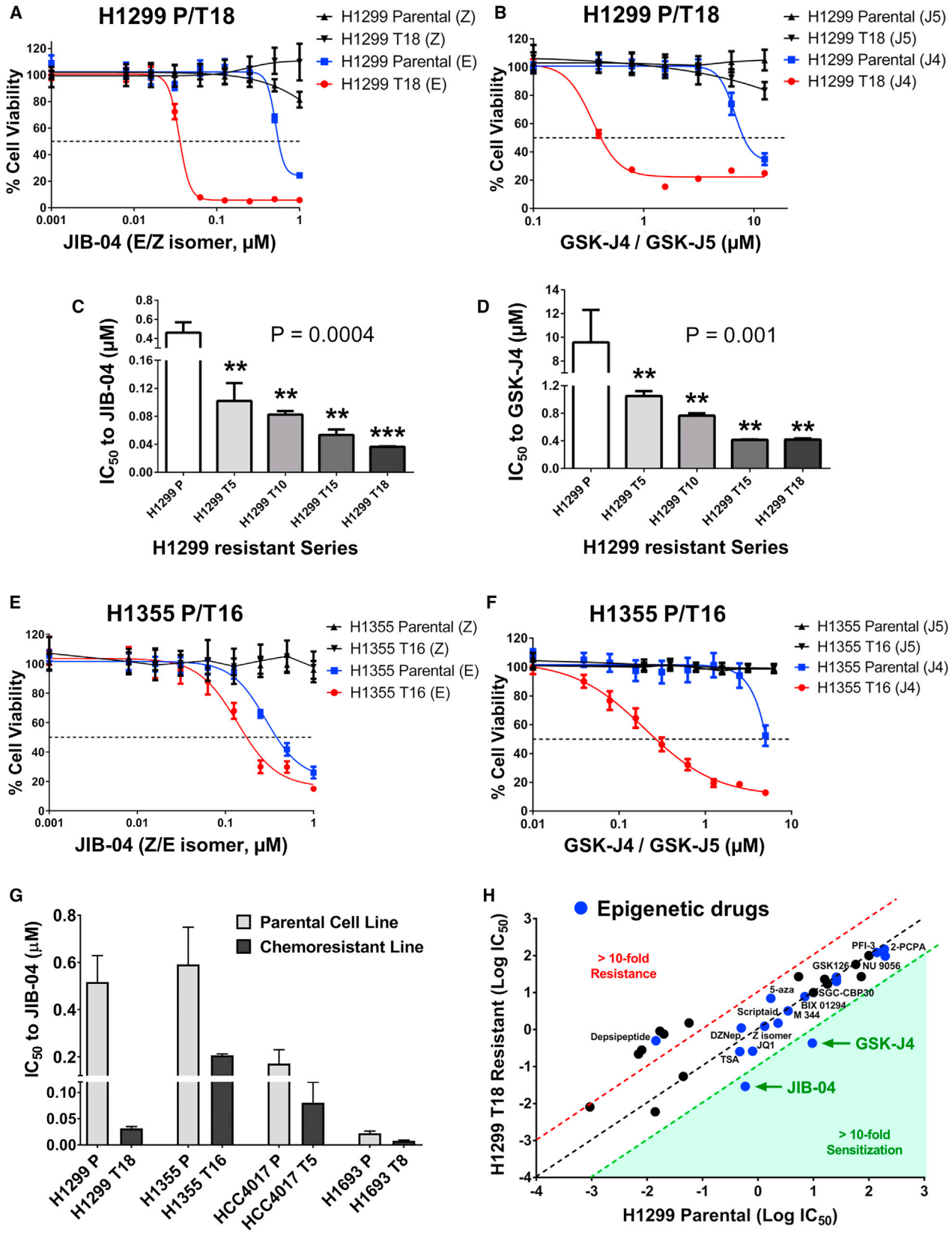


*(legend on next page)*

to GSK-J4 than parental cells, and there was no effect on cell viability with the inactive GSK-J5 (Figure 4B).

To investigate whether increased KDM expression and pharmacological sensitivity to JmjC inhibitors accompanied the progressive increase in chemoresistance, we queried the entire H1299 resistant series. In agreement with increased KDM upregulation (Figure 3D), we saw a consistent decrease in $IC_{50}$ values to JIB-04 and GSK-J4 as cells progressed from H1299 parental to the H1299 T18 variant (Figures 4C and 4D).

To explore the generality of increased sensitivity of taxane-platin-resistant NSCLC cells to JmjC inhibitors, we tested other resistant cell line variants. H1355 T16, which had upregulation of KDM3B and KDM6A (Figure S4B), showed higher sensitivity to JIB-04 (Figure 4E) and GSK-J4 (Figure 4F) than H1355 parental. Other taxane-platin-resistant cell lines, including HCC4017 T5 and H1693 T8, were also more sensitive to JIB-04 than their corresponding parental cells (Figures 4G, S5A, and S5B), with a fold-sensitivity proportional to their level of taxane-platin resistance. Of note, HCC4017 and H1693 parental cell lines were already highly sensitive to the KDM5/KDM6-specific inhibitor GSK-J4 (Figure S5C). Their HCC4017-T5- and H1693-T8-resistant variants, although hypersensitized to JIB-04, did not show any further reduction in GSK-J4 $IC_{50}$ values (Figure S5C), suggesting that these cells may have acquired resistance independently of H3K4 or H3K27me3 demethylases. Indeed, qRT-PCR analysis revealed modest upregulation of other KDMs in HCC4017 T5 and H1693 T8 (Figures S5D and S5E), including known JIB-04 targets (Wang et al., 2013).

To evaluate if the hypersensitivity of taxane-platin-resistant cells was specific to JmjC KDM inhibitors or represented a general epigenetic susceptibility, we tested other compounds inhibiting 2-OG oxygenases, histone methyltransferases (HMTs), LSD1 demethylase, histone acetyltransferases (HATs), histone deacetylases (HDACs), DNA methyltransferases (DNMTs), or bromodomains (BRDs). We did not see significant differences in $IC_{50}$ values of any of these drugs between parental cells and taxane-platin-resistant variants (Figures 4H and S6; Table S6). Of particular note was the lack of hypersensitivity to HMT inhibitors and 2-OG oxygenase inhibitors (Table S6), consistent with no general expression changes in these enzyme families (GEO: GSE77209). Our studies have thus uncovered a specific, targetable epigenetic vulnerability to Jumonji inhibition that can be exploited to treat NSCLCs that develop resistance to taxane-platin chemotherapy.

## JIB-04 or GSK-J4 Treatment Results in Reversal of a Subset of Transcriptional Programs Deregulated in Taxane-Platin-Resistant Cells

In agreement with the hypersensitivity of chemoresistant cells to JmjC inhibitors, we observed that short-term (24-hr) treatment with 0.2 μM JIB-04 (Figures S7A and S7B) or 1 μM GSK-J4 (Figures S7C and S7D) led to gene expression changes selectively in H1299-T18-resistant cells with minimal transcriptional changes in H1299 parental cells ($p \leq 0.05$). Importantly, JmjC inhibitor treatment of H1299 T18 partially reversed expression changes acquired during the development of taxane-platin resistance (Figures S7E and S3F; Table S7). Furthermore, gene set enrichment analysis (GSEA) using curated gene sets from molecular signatures database (MSigDB) (Subramanian et al., 2005) revealed reversal of a subset of transcriptional programs in H1299 T18 cells upon JmjC inhibitor treatment, with a significant overlap between JIB-04 and GSK-J4 (Figure 5A). Out of the 214 gene sets that were depleted after resistance development in H1299 T18 cells, 38 gene sets (~20%) were enriched (reversed) by both JIB-04 and GSK-J4. These 38 overlapping gene sets (Table S8) included functionally relevant categories such as genes with H3K4me3 and H3K27me3 marks (MSigDB, M1941; Meissner et al., 2008; shown in Figure 5A, left), as well as SUZ12 ChIP-on-chip targets, indicative of genes regulated by H3K27me3 (MSigDB, M9898; Table S8; Ben-Porath et al., 2008). Also included in the overlap were apoptotic gene sets such as MDM4 target genes, TP63 target genes, and TP53 target genes (Table S8). A gene set representing genes upregulated in apoptotic tissues (MSigDB, M5681; Martoriati et al., 2005) enriched by both JmjC inhibitors is shown in Figure 5A (right).

To gain insights into the H3K4me3 and H3K27me3 dynamics revealed by GSEA (Figure 5A, left), we performed detailed promoter bivalency analyses of our ChIP-seq data. We first identified H3K4me3 and H3K27me3 bivalent gene promoters in H1299 parental and H1299 T18 cells. Genes were classified as bivalent if both H3K4me3 and H3K27me3 were ≥4-fold over input in the TSS ±500 bp region. We found that there was an overall decrease in the total number of bivalent genes in H1299 T18 compared to parental cells (Figure 5B, bar graph). A great majority of these genes (~80%) showed at least a 2-fold signal loss. We next classified the "bivalency lost" genes by loss of H3K4me3, loss of H3K27me3, or loss of both marks (Figure 5B, pie chart). Many of the genes that had lost their bivalency in H1299 T18, compared to H1299 parental, re-gained these marks

**Figure 4. Chemoresistant Cell Lines Show Increased Sensitivity to JmjC KDM Inhibitors**

(A and B) H1299 T18 cells showed hypersensitivity to JIB-04 active "E" isomer (A) as well as GSK-J4 (B), compared to H1299 parental. Inactive drug isomers (JIB-04 "Z" isomer and GSK-J5) had no effect. Each data point represents mean ± SD from eight replicates per drug dose.

(C and D) $IC_{50}$ plots for H1299-resistant series for response to JIB-04 (C) and GSK-J4 (D). Data represent mean ± SD. Statistical significance was tested by one-way ANOVA, followed by Dunnett's multiple comparisons with H1299 parental (**$p < 0.01$, ***$p < 0.001$). p values listed on graphs are from post-test for linear trend.

(E and F) H1355-T16-resistant variant was hypersensitized to JIB-04 active E isomer (E) and GSK-J4 (F), but not to inactive isomers, compared to H1355 parental. Each data point represents mean ± SD from eight replicates per drug dose.

(G) $IC_{50}$ values show general hypersensitivity of H1299 T18, H1355 T16, HCC4017 T5, and H1693 T8 to JIB-04. Data represent mean ± SEM. p values are from two-way ANOVA ($p < 0.01$).

(H) $Log_{10}$ $IC_{50}$ values for standard, targeted and epigenetic drugs for H1299 T18 chemoresistant versus H1299 Parental cells. Epigenetic drugs (blue dots) include inhibitors of KDM, LSD1, HMT, HDAC, HAT, DNMT, and BRD. The red dotted line denotes the 10-fold cut-off for cross-resistance, and the green dotted line is the 10-fold cut-off for sensitization.

See also Figures S5 and S6 and Table S6.

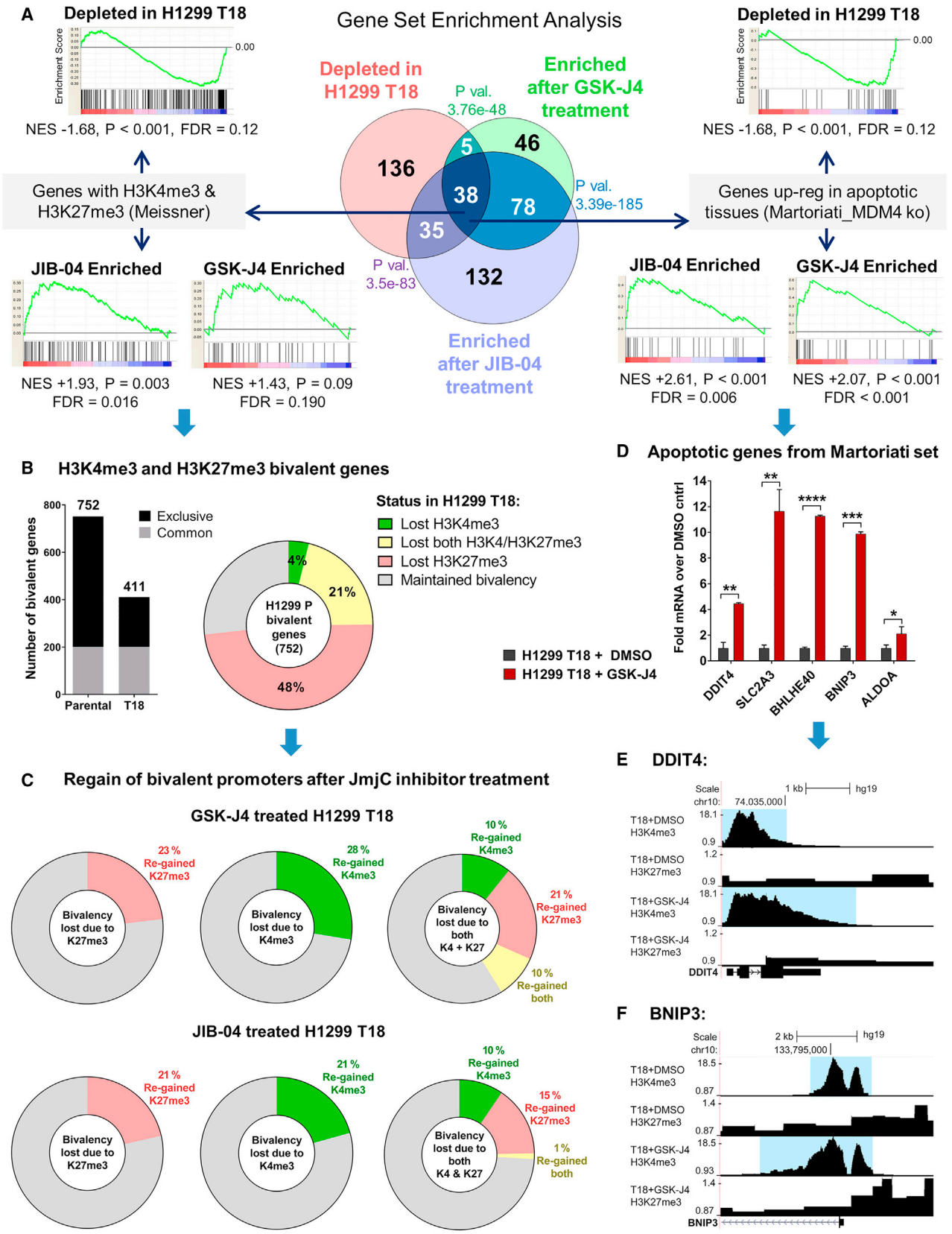


(legend on next page)

(at least a 1.5-fold increase) after short-term GSK-J4 or JIB-04 treatment of T18 cells (shown by category in Figure 5C).

To validate the apoptotic gene set enrichment uncovered by GSEA on our microarray data, we queried known apoptotic genes from the Martoriati gene set (Figure 5A, right) in our RNA-seq dataset. As shown in Figure 5D, pro-apoptotic genes were significantly upregulated by short-term JmjC inhibitor treatment of T18 cells. Additionally, these and some other pro-apoptotic/anti-proliferative genes were confirmed by qRT-PCR to be upregulated by both JIB-04 and GSK-J4, whereas proliferative/oncogenic genes were significantly downregulated in JmjC-inhibitor-treated T18 cells (Figure S8A). ChIP-seq traces of sample pro-apoptotic genes upregulated by JmjC inhibitors, DDIT4 and BNIP3 are shown in Figures 5E and 5F, respectively, exhibiting greater enrichment of the H3K4me3 activating mark. In contrast, histone marks at the MDR1 locus were not altered by JmjC inhibitor treatment, nor was MDR1 expression, as expected from its genetic amplification (Figures S8B–S8F).

These analyses confirmed that major changes in the H3K4me3/H3K27me3 dynamics accompany the development of chemoresistance and that short-term JmjC inhibitor treatment can partly reverse these changes, killing drug-resistant cells with high potency.

## Chemoresistant Tumors Show Increased Response to GSK-J4 and JIB-04 In Vivo

To evaluate the response of taxane-platin-chemoresistant NSCLC cells to JmjC inhibitors in vivo, we established subcutaneous xenografts of H1299 parental and H1299 T18 cells and compared their response to GSK-J4 or JIB-04. GSK-J4 caused a significant reduction in tumor volumes selectively in H1299 T18 xenografts ($p < 0.0001$) (Figure 6A and 6B). Treated T18 tumors also showed a significant decrease in final tumor weights ($p < 0.01$) (Figure 6B, right), without mice body weight loss (Figure S9A). For the JIB-04 study, tumor-bearing mice were randomized to receive 5 mg/kg, 20 mg/kg, or 50 mg/kg treatment or vehicle. At all doses, JIB-04 resulted in greater percent reduction in final tumor volumes of H1299 T18 compared to H1299 parental (Figures 6C and 6D). JIB-04 treatment preferentially slowed T18 tumor growth and decreased tumor growth rate, as seen by increased tumor doubling times (Figure 6E), without any toxicity on treated mice (Figure S9A).

To evaluate whether the targeted KDM enzymatic activity was reduced in the JmjC-inhibitor-treated tumors in vivo, we measured histone demethylase activity in drug versus vehicle treated tumor lysates by ELISA. Chemoresistant H1299 T18 xenografts had higher H3K4me3, H3K9me3, and H3K27me3 demethylase activity than H1299 parental tumors (Figure 6F), in agreement with increased KDM expression. KDM6 inhibitor GSK-J4 significantly inhibited H3K27me3 demethylase activity in H1299 T18 xenografts (Figure 6F, right), without reducing H3K4me3 or H3K9me3 demethylase activity (Figure 6F, left and middle). The pan-JmjC inhibitor JIB-04 significantly inhibited H3K4me3, H3K9me3, and H3K27me3 demethylase activity in H1299 T18 xenografts (Figure 6G). In addition, we saw evidence of cytostatic/cytotoxic effects in JmjC-inhibitor-treated chemoresistant xenografts (Figures S9C–S9E).

We then validated the hypersensitivity of chemoresistant tumors to JIB-04 and GSK-J4 in an additional in vivo model, comparing treatment response in H1355 parental versus H1355 T16. JmjC-inhibitor-treated H1355 parental xenografts continued to grow in volume throughout the 28 days of treatment (Figure 6H, left), whereas treated H1355 T16 tumors exhibited significant tumor shrinkage (Figure 6H, right). No appreciable toxicity was seen in JIB-04- or GSK-J4-treated mice (Figure S9B). Both in vivo models confirmed the increased sensitivity of taxane-platin-chemoresistant tumors to JIB-04 and GSK-J4. Taken together, these data provide proof of principle for the use of JmjC inhibitors to target drug-resistant NSCLCs.

## JmjC KDM Inhibitors Synergize with Taxane-Platin Standard Chemotherapy and Prevent Emergence of Drug Tolerance

Given the hypersensitivity of chemoresistant cells to JmjC inhibitors and the transcriptional reprogramming seen in resistant cells, we asked whether JIB-04 or GSK-J4 would synergize with taxane-platin chemotherapy in killing chemoresistant clones. Using JIB-04 or GSK-J4 doses that were predetermined to not cause complete growth inhibition as single agents, both of these drugs were effective in synergistically inhibiting

**Figure 5. JIB-04 and GSK-J4 Cause Reversal of Deregulated Transcriptional Programs, Regain of H3K4me3-H3K27me3 Promoter Bivalency, and Induction of Pro-apoptotic Genes in Chemoresistant Cells**

(A) GSEA of differentially expressed gene lists from microarray against MSigDB curated gene sets revealed transcriptional programs that were depleted in H1299-T18-resistant versus H1299 parental cells are enriched by 24-hr treatment with JIB-04 (0.2 μM) or GSK-J4 (1 μM). p values signify overlap by hypergeometric tests. Two of the 38 overlapping gene sets are shown. Left: genes with H3K4me3 and H3K27me3 (Meissner et al., 2008; M1941), Right: genes upregulated in apoptotic tissues (Martoriati et al., 2005; M5681). NES, normalized enrichment score. p values under GSEA plots are nominal p values.

(B) ChIP-seq analysis confirmed loss of bivalent genes in H1299 T18 versus parental cells. Number of bivalent genes (bar graph) and breakdown by lost or gain of marks (pie) are shown.

(C) Genes in each of the bivalency lost categories depicted in the pie chart in (B) were probed for their regain status (at least a 1.5-fold increase) in GSK-J4- and JIB-04-treated H1299 T18 cells.

(D) Genes from the Martoriati et al. apoptotic gene set identified in (A) were confirmed to be upregulated by GSK-J4 by RNA-seq. Error bars indicate mean ± SEM from biological duplicates. Significance was tested using the powerful FDR (q) approach of two-stage linear step-up procedure of Benjamini, Krieger, and Yekutieli; *$q < 0.05$, **$q < 0.01$, ***$q < 0.001$, ****$q < 0.0001$.

(E) ChIP-seq traces for the pro-apoptotic, upregulated gene DDIT4, showing increased H3K4me3 (blue highlight) in GSK-J4- versus DMSO-treated H1299 T18 cells.

(F) ChIP-seq traces for BNIP3 upregulated gene, showing broader H3K4me3 enrichment in GSK-J4-treated versus DMSO-treated H1299 T18 cells. GSK-J4: 1 μM, 24 hr (for both E and F).

See also Figures S7 and S8 and Tables S7 and S8.

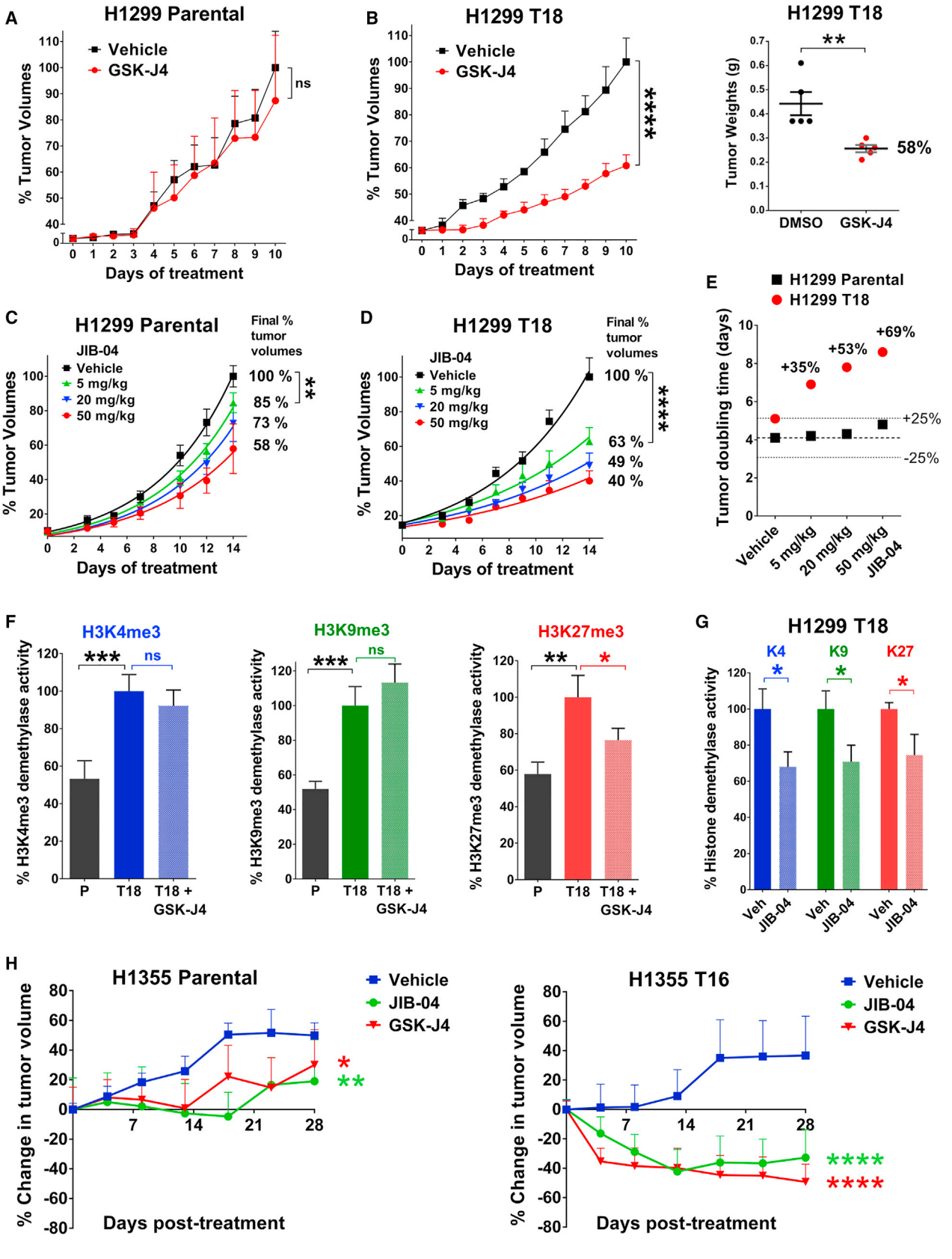


(legend on next page)

H1299-T18-chemoresistant colonies surviving taxane-platin treatment (indicated by positive delta Bliss in Figures 7A and 7B).

We also investigated blocking the emergence of drug-tolerant colonies from taxane-platin-sensitive, chemo-naive cell lines. H1299 parental cells were exposed to paclitaxel-carboplatin under conditions that allowed for a surviving subpopulation. We then evaluated the impact of sublethal doses of various epigenetic compounds in inhibiting colony forming ability of these taxane-platin "persister" cells (Figure 7C). Only the JmjC inhibitor prevented the emergence of drug-tolerant colonies from H1299 parental cells, whereas inhibitors of other epigenetic enzymes did not (Figure 7C). Next, we assessed if JmjC inhibition could block the outgrowth of persister colonies from other chemosensitive NSCLC cell lines. H1355, HCC4017, and H1693 parental cells were exposed to their respective predetermined paclitaxel-carboplatin doublet concentrations that allowed for a surviving subpopulation. Sublethal doses of GSK-J4 inhibited the outgrowth of these taxane-platin drug-tolerant colonies (Figure 7D).

We therefore evaluated the impact of JmjC inhibitors in combination with standard taxane-platin chemotherapy in vivo. Combination of JIB-04 or GSK-J4 with paclitaxel-carboplatin chemotherapy resulted in significantly greater tumor growth inhibition of H1299 parental xenografts than single agents and gave a synergistic response (Figure 7E, top, positive delta Bliss). There was a significant reduction in tumor burden compared to either therapy alone (Figure 7E bottom, tumor weights), without general toxicity.

Our results thus present a new therapeutic opportunity for not only targeting of NSCLCs after development of drug resistance but also possibly preventing the emergence of chemoresistant subpopulations and achieving greater response in chemosensitive lung cancers treated with standard taxane-platin chemotherapy.

## DISCUSSION

We have established preclinical models of NSCLC resistance to taxane-platin doublet chemotherapy and identified upregulation of JmjC histone lysine demethylases as an underlying epigenetic change co-developing with increasing chemoresistance and leading to progressive sensitization to JmjC KDM inhibitors. These findings define JmjC demethylases as promising therapeutic targets in drug-resistant NSCLCs and for potentially preventing the emergence of taxane-platin drug tolerance.

Our work suggests that NSCLC cells may dynamically express multiple JmjC KDMs, in line with recent similar observations in glioblastoma (Liau et al., 2017). Further, KDMs may have a role not only in survival from the first drug contact but also in maintaining transcriptional plasticity and increasing epigenetic alterations during the progression toward robust drug resistance. Chemoresistant cells appear to be epigenetically addicted, becoming specifically hypersensitized to JmjC KDM inhibitors. Future genetic studies will need to determine which JmjC demethylases are the key mediators of this phenotype.

Due to their ability to regulate multiple transcriptional programs at once, epigenetic mechanisms might serve to restore the cellular signaling balance (Mair et al., 2014) that is perturbed by chemotherapy stress, acting as a defense mechanism to protect cells from further insults. It is unclear if JmjC-enzyme-overexpressing subpopulations exist in the original population or are acquired de novo, upon selective pressure. Our studies suggest that the resistance is likely manifested as a combination of both intrinsic and acquired changes. While GSK-J4 eliminated the emergence of drug-resistant colonies in a short-term colony formation assays, our long-term drug treatment studies revealed that resistant cells were also acquiring permanent/genetic changes over time, nevertheless maintaining their hypersensitivity to JmjC inhibitors.

Since our previous studies have shown that normal human bronchial epithelial cells are not sensitive to JmjC inhibition (Wang et al., 2013), our findings suggest that there is a therapeutic window for lung cancer therapy, while also raising the possibility of extending the utility of JmjC inhibitors to other drug-resistant solid tumors. Pharmacological targeting of JmjC KDMs could help prevent the development of drug resistance while also providing a therapeutic option to treat chemoresistant tumors.

**Figure 6. JmjC-Inhibitor-Treated Chemoresistant Tumors Have Lower Histone Demethylase Activity and Increased Response to GSK-J4 and JIB-04 In Vivo**

(A and B) GSK-J4 treatment significantly reduced final tumor burden of H1299 T18 xenografts (B); response in H1299 parental xenografts was not significant (A). The y axis depicts percent tumor volumes normalized to average vehicle tumor volume at the end of treatment. Data represent mean ± SEM; n = 5 mice per group. p values for tumor volume growth are from two-way ANOVA (ns, not significant, ****$p < 0.0001$). Tumor weights (B, right) were compared using an two-tailed unpaired t test (**$p = 0.007$).

(C and D) At all doses, JIB-04 caused a greater percent reduction in H1299 T18 tumor volumes (D) than in H1299 parental tumors (C). Data represent mean ± SEM; n = 6–8 mice per group. The y axis depicts percent tumor volumes normalized to average vehicle tumor volume on day 14. Exponential growth curves were fitted using non-linear regression. Drug response was compared using a two-way ANOVA. For the 5 mg/kg versus vehicle group in H1299 parental, **$p = 0.001$, and for H1299 T18, ****$p < 0.0001$.

(E) JIB-04 treatment slowed tumor growth and increased doubling time of treated H1299 T18 tumors by 69%, with minimal effect on H1299 parental tumors (<25% change). Doubling times were derived from exponential growth curves in (C) and (D).

(F) H3K4me3/H3K9me3/K27me3 demethylase activity in tumor lysates from GSK-J4-treated mice. p values are from Fisher's LSD test post one-way ANOVA (*$p < 0.1$, **$p < 0.01$, ***$p < 0.001$).

(G) JIB-04 treated H1299 T18 xenografts showed significant reduction in H3K4me3, H3K9me3, and H3K27me3 demethylase activity. p values are from two-tailed unpaired t tests (*$p \leq 0.05$).

(H) Percent change in tumor volumes relative to the treatment start volume (~120 $mm^3$) is shown for H1355 parental (left) and H1355 T16 (right) xenografts. p values are from two-way ANOVA (*$p < 0.05$, **$p < 0.01$, ****$p < 0.0001$).

See also Figure S9.

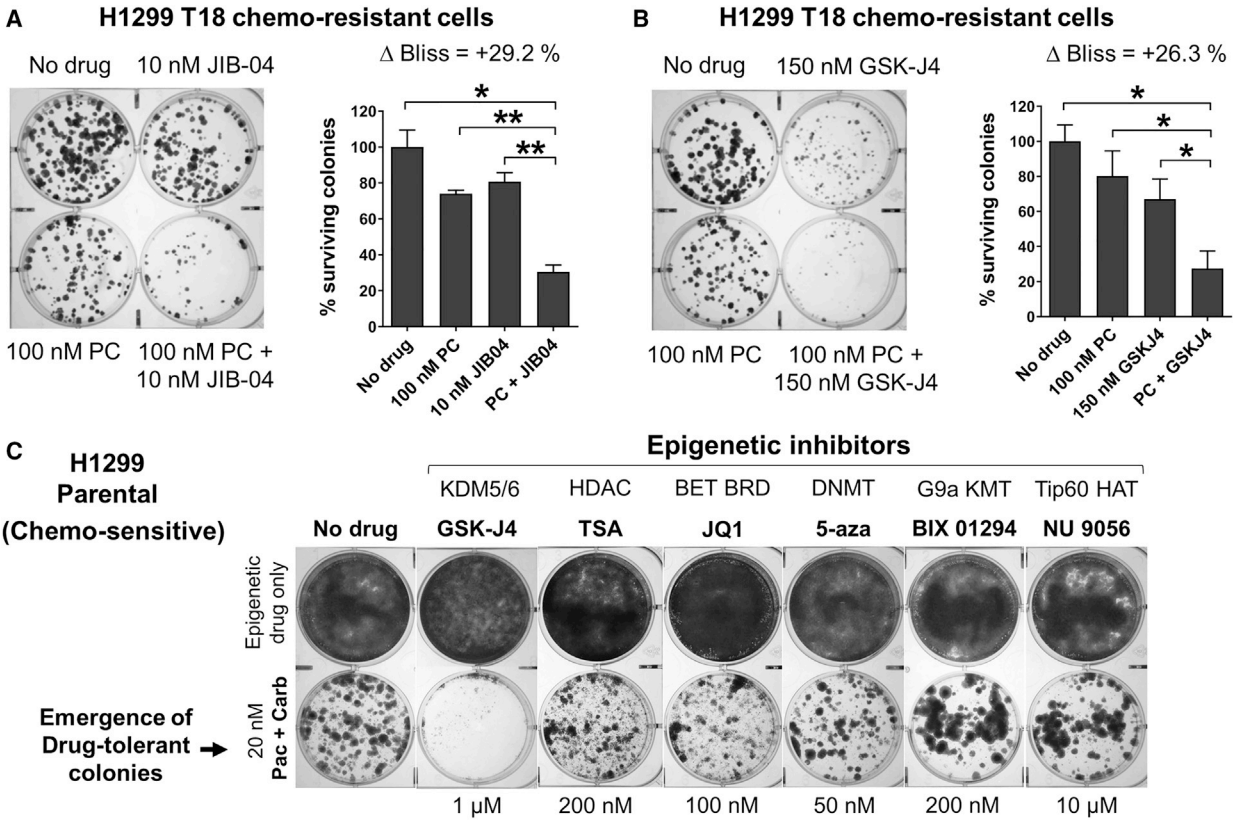


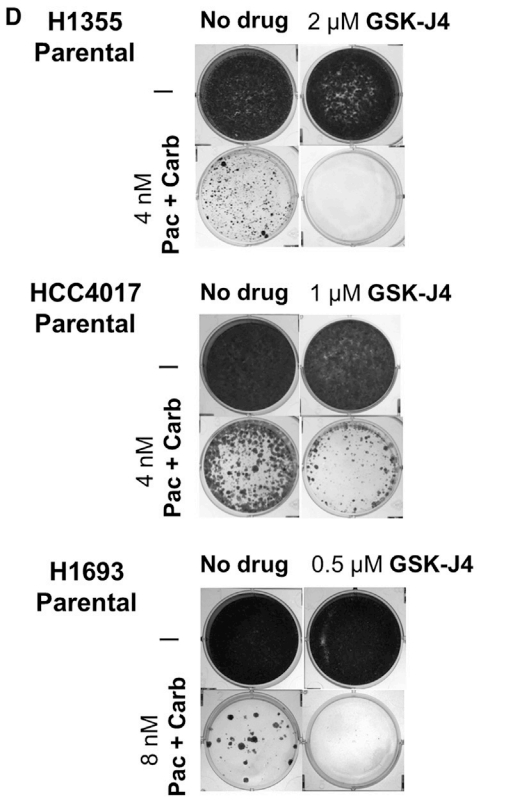


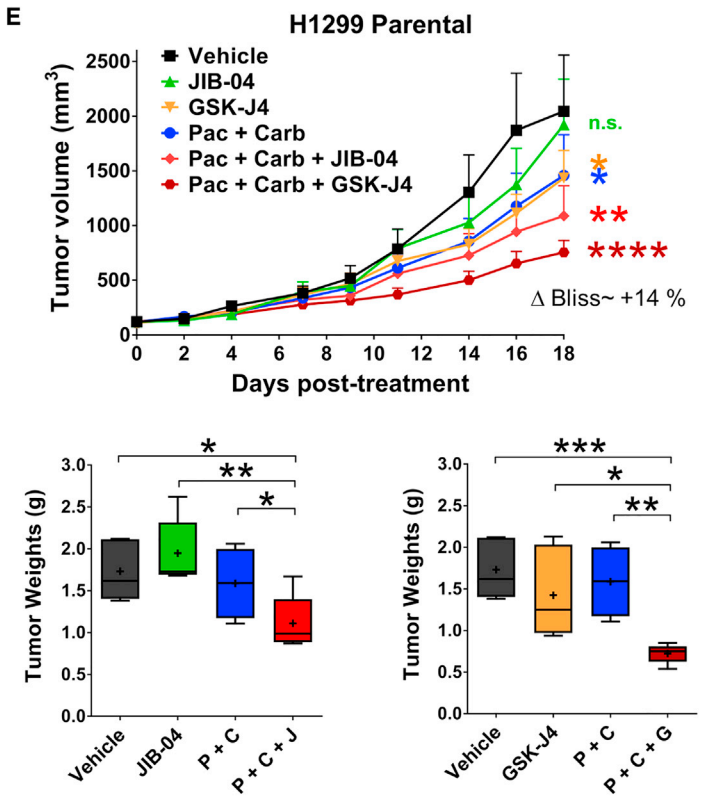


*(legend on next page)*

## EXPERIMENTAL PROCEDURES

### Cell Lines

NSCLC lines were obtained from the Hamon Cancer Center Collection (University of Texas Southwestern Medical Center). Cell lines were DNA fingerprinted using PowerPlex 1.2 kit (Promega) and confirmed to be mycoplasma-free using e-Myco kit (Boca Scientific). Cells were maintained in RPMI-1640 (Life Technologies) with 5% FBS at 37°C in a humidified atmosphere containing 5% $CO_2$.

### In Vitro Drug Assays

NSCLC lines were treated with paclitaxel-carboplatin combination, given in a ~2:3 w/w ratio, to mirror the clinical dosage values of 225 mg/m$^2$ paclitaxel and 330 mg/m$^2$ carboplatin. Considering the molecular weights of the two drugs, this translates to an ~1:3.4 molar ratio. Drugs were given in cycles, consisting of 4–5 days of drug treatment and 1–2 weeks of drug-free culturing to allow the surviving cells to repopulate. Treatment was started with 2×–3× $IC_{50}$ doses, and doses were increased with increasing treatment cycles, ultimately reaching ~30×–50× $IC_{50}$, depending on the cell line. Untreated parental cells were maintained at all times for comparison. Cell viability after 4-day treatments was assessed in 96-well plates using standard 3-(4,5-dimethylthiazol-2-yl)-5-(3-carboxymethoxyphenyl)-2-(4-sulfophenyl)-2H-tetrazolium, inner salt (MTS) assays (Promega). Drugs were tested in serial dilutions, totaling eight different drug concentrations, with eight replicates per concentration. Response was validated in replicate plates ($n \geq 3$).

### In Vivo Studies

Animals were housed under standard, sterile conditions at The University of Texas Southwestern (UTSW) animal facility. All experiments were carried out under approved Institutional Animal Care and Use Committee (IACUC) protocols and followed UTSW animal care procedures. Experimental details are provided in Supplemental Experimental Procedures.

### Patient Tumors

Human specimens and clinical data were used after full de-identification under MD Anderson institutional review board (IRB)-approved/exempted protocols. This included both chemo-naive and neoadjuvant-treated tumors and complete histopathological and clinical annotation. Fresh frozen tumor samples from the time of resection were used for Illumina gene expression profiling, and some were formalin-fixed, paraffin-embedded (FFPE) tumors for tissue microarrays.

### Microarrays

Gene expression profiling was performed using Illumina HumanWG-6 V3 BeadArrays (for NSCLC patient tumors) or Illumina Human HT-12 V4 BeadArrays (for cell lines, xenografts). Cell line and xenograft microarrays included biological replicates (cell lines: five for parental, three for most resistant variant, and two for each intermediate time point; xenografts: three tumors each for parental and resistant group). Data were pre-processed using the R package mbcb for background correction (Ding et al., 2008) and then log-transformed and quantile-normalized with the R package preprocessCore or using in-house MATRIX software (microarray transformation in Excel). See Supplemental Experimental Procedures for microarray analysis details.

### Statistical Methods

All statistical tests were performed using GraphPad Prism 6/7. Dose-response curves and $IC_{50}$ values were also calculated using in-house DIVISA (database of in vitro sensitivity assays; L.G., unpublished data). For synergy estimation, ΔBliss excess was calculated as shown previously (Wilson et al., 2014). Bliss expectation was calculated as $A + B - (A \times B)$, where A and B denote the fractional responses from drugs A and B given individually. The difference between Bliss expectation and observed response from combination of drugs A and B at the same doses is the ΔBliss excess.

## ACCESSION NUMBERS

The accession numbers for the microarray data and ChIP-seq and RNA-seq datasets reported in this paper are GEO: GSE77209 and GEO: GSE81689, respectively.

## SUPPLEMENTAL INFORMATION

Supplemental Information includes Supplemental Experimental Procedures, nine figures, eight tables, and one data file and can be found with this article online at http://dx.doi.org/10.1016/j.celrep.2017.04.077.

## AUTHOR CONTRIBUTIONS

M.P.D. designed and performed experiments, analyzed data, and wrote the manuscript. L.W., H.P., J.B., and B.T. helped with in vivo experiments. R.Z., Y.Z., K.C., Y.X., and L.G. helped in microarray data analysis. R.K.K., P.Y., and R.K. performed ChIP experiments and bioinformatics analysis. N.V.B. and B.A.G. performed histone post-translational modification (PTM) mass spectrometry. J.R.-C., C.B., B.M., P.V., E.R.P., M.S., A.P., S.G.S., N.K., J.V.H., A.F.G., and I.I.W. provided clinically annotated patient dataset or pathological data. J.D.M. contributed to project design and manuscript edits. E.D.M. designed and guided the project and co-wrote and edited the manuscript.

## ACKNOWLEDGMENTS

The authors thank current and past members of Minna and Martinez laboratories for assistance, particularly Michael Peyton, Amit Das, Boning Gao, and Nicholas Levonyak. We are thankful to Dr. Michael Roth and Dr. Jerry Shay (UT Southwestern) for helpful discussions. Research reported in this publication was partly funded by the National Cancer Institute (NCI) (grant R01 CA125269 to E.D.M., grant P50CA70907 to J.D.M., and grant P01 CA196539 to B.A.G.), the Department of Defense (grants W81XWH-07-1-0306 and W81XWH-16-1-0129), CPRIT (grants RP160493, RP120717, and RP110708), the Friends of the Cancer Center (E.D.M.), The Welch Foundation (grant I-1878 to E.D.M.), and an LLS Robert Arceci Scholar Award (to B.A.G.). We also recognize the support to UT Southwestern Simmons Cancer Center

**Figure 7. JmjC KDM Inhibitors Synergize with Paclitaxel-Carboplatin Standard Chemotherapy in Blocking Emergence of Drug Tolerance from Chemosensitive NSCLCs In Vitro and In Vivo**

(A and B) Combination of JIB-04 (A) or GSK-J4 (B) with standard paclitaxel-carboplatin chemotherapy synergistically inhibited colony formation from H1299 T18. Error bars represent mean ± SD from duplicate assays. p values are from two-tailed unpaired t tests (*$p < 0.1$, **$p < 0.01$). Response was greater than additive, indicated by positive ΔBliss.

(C) Sublethal doses of the JmjC KDM inhibitor GSK-J4 (but not other epigenetic inhibitors) prevented the emergence of paclitaxel-carboplatin drug-tolerant colonies from chemosensitive H1299 parental. Representative images from replicate assays (n = 3) are shown.

(D) GSK-J4 also blocked the emergence of paclitaxel-carboplatin drug-tolerant colonies from other chemosensitive NSCLC cell lines: H1355, HCC4017, and H1693.

(E) H1299 Parental tumor volumes during in vivo combination treatment are shown in the top panel and tumor weights at sacrifice in the bottom graphs. Statistical tests on tumor volumes represent comparison of each treatment group with the vehicle group by two-way ANOVA (n.s., not significant; *$p < 0.05$, **$p < 0.01$, ****$p < 0.0001$). ΔBliss for (Pac + Carb + JIB-04) combination = +13.8%; ΔBliss for (Pac + Carb + GSK-J4) = +13.9%. Both values indicate synergy. p values for tumor weight comparisons are from two-tailed unpaired t tests (*$p < 0.1$, **$p < 0.01$, ***$p < 0.001$).

Shared Resources by the NCI of the National Institutes of Health (grant 5P30CA142543) and to MD Anderson Institutional Tissue Bank, ITBS (grant 2P30CA016672).

Received: October 27, 2015
Revised: March 6, 2017
Accepted: April 27, 2017
Published: May 23, 2017

## REFERENCES

American Cancer Society (2015). Cancer Facts & Figures. American Cancer Society, Inc.. https://www.cancer.org/content/dam/cancer-org/research/cancer-facts-and-statistics/annual-cancer-facts-and-figures/2015/cancer-facts-and-figures-2015.pdf

Ben-Porath, I., Thomson, M.W., Carey, V.J., Ge, R., Bell, G.W., Regev, A., and Weinberg, R.A. (2008). An embryonic stem cell-like gene expression signature in poorly differentiated aggressive human tumors. Nat. Genet. *40*, 499–507.

Bradshaw, D.M., and Arceci, R.J. (1998). Clinical relevance of transmembrane drug efflux as a mechanism of multidrug resistance. J. Clin. Oncol. *16*, 3674–3690.

Busschots, S., O'Toole, S., O'Leary, J.J., and Stordal, B. (2015). Carboplatin and taxol resistance develops more rapidly in functional BRCA1 compared to dysfunctional BRCA1 ovarian cancer cells. Exp. Cell Res. *336*, 1–14.

d'Amato, T.A., Landreneau, R.J., Ricketts, W., Huang, W., Parker, R., Mechetner, E., Yu, I.R., and Luketich, J.D. (2007). Chemotherapy resistance and oncogene expression in non-small cell lung cancer. J. Thorac. Cardiovasc. Surg. *133*, 352–363.

Ding, L.H., Xie, Y., Park, S., Xiao, G., and Story, M.D. (2008). Enhanced identification and biological validation of differential gene expression via Illumina whole-genome expression arrays through the use of the model-based background correction methodology. Nucleic Acids Res. *36*, e58.

Gottesman, M.M., Fojo, T., and Bates, S.E. (2002). Multidrug resistance in cancer: role of ATP-dependent transporters. Nat. Rev. Cancer *2*, 48–58.

Howlader, N., Noone, A.M., Krapcho, M., Garshell, J., Miller, D., Altekruse, S.F., Kosary, C.L., Yu, M., Ruhl, J., Tatalovich, Z., et al. (1975–2012). SEER Cancer Statistics Review (National Cancer Institute).

Kim, J.Y., Kim, K.B., Eom, G.H., Choe, N., Kee, H.J., Son, H.J., Oh, S.T., Kim, D.W., Pak, J.H., Baek, H.J., et al. (2012). KDM3B is the H3K9 demethylase involved in transcriptional activation of lmo2 in leukemia. Mol. Cell. Biol. *32*, 2917–2933.

Knoechel, B., Roderick, J.E., Williamson, K.E., Zhu, J., Lohr, J.G., Cotton, M.J., Gillespie, S.M., Fernandez, D., Ku, M., Wang, H., et al. (2014). An epigenetic mechanism of resistance to targeted therapy in T cell acute lymphoblastic leukemia. Nat. Genet. *46*, 364–370.

Kruidenier, L., Chung, C.W., Cheng, Z., Liddle, J., Che, K., Joberty, G., Bantscheff, M., Bountra, C., Bridges, A., Diallo, H., et al. (2012). A selective jumonji H3K27 demethylase inhibitor modulates the proinflammatory macrophage response. Nature *488*, 404–408.

Lemontt, J.F., Azzaria, M., and Gros, P. (1988). Increased mdr gene expression and decreased drug accumulation in multidrug-resistant human melanoma cells. Cancer Res. *48*, 6348–6353.

Liau, B.B., Sievers, C., Donohue, L.K., Gillespie, S.M., Flavahan, W.A., Miller, T.E., Venteicher, A.S., Hebert, C.H., Carey, C.D., Rodig, S.J., et al. (2017). Adaptive chromatin remodeling drives glioblastoma stem cell plasticity and drug tolerance. Cell Stem Cell *20*, 233–246.

Mair, B., Kubicek, S., and Nijman, S.M. (2014). Exploiting epigenetic vulnerabilities for cancer therapeutics. Trends Pharmacol. Sci. *35*, 136–145.

Martin, J., Ginsberg, R.J., Venkatraman, E.S., Bains, M.S., Downey, R.J., Korst, R.J., Kris, M.G., and Rusch, V.W. (2002). Long-term results of combined-modality therapy in resectable non-small-cell lung cancer. J. Clin. Oncol. *20*, 1989–1995.

Martoriati, A., Doumont, G., Alcalay, M., Bellefroid, E., Pelicci, P.G., and Marine, J.C. (2005). dapk1, encoding an activator of a p19ARF-p53-mediated apoptotic checkpoint, is a transcription target of p53. Oncogene *24*, 1461–1466.

Massarelli, E., Andre, F., Liu, D.D., Lee, J.J., Wolf, M., Fandi, A., Ochs, J., Le Chevalier, T., Fossella, F., and Herbst, R.S. (2003). A retrospective analysis of the outcome of patients who have received two prior chemotherapy regimens including platinum and docetaxel for recurrent non-small-cell lung cancer. Lung Cancer *39*, 55–61.

Meissner, A., Mikkelsen, T.S., Gu, H., Wernig, M., Hanna, J., Sivachenko, A., Zhang, X., Bernstein, B.E., Nusbaum, C., Jaffe, D.B., et al. (2008). Genome-scale DNA methylation maps of pluripotent and differentiated cells. Nature *454*, 766–770.

Roesch, A., Vultur, A., Bogeski, I., Wang, H., Zimmermann, K.M., Speicher, D., Körbel, C., Laschke, M.W., Gimotty, P.A., Philipp, S.E., et al. (2013). Overcoming intrinsic multidrug resistance in melanoma by blocking the mitochondrial respiratory chain of slow-cycling JARID1B(high) cells. Cancer Cell *23*, 811–825.

Roninson, I.B., Chin, J.E., Choi, K.G., Gros, P., Housman, D.E., Fojo, A., Shen, D.W., Gottesman, M.M., and Pastan, I. (1986). Isolation of human mdr DNA sequences amplified in multidrug-resistant KB carcinoma cells. Proc. Natl. Acad. Sci. USA *83*, 4538–4542.

Scagliotti, G.V., Parikh, P., von Pawel, J., Biesma, B., Vansteenkiste, J., Manegold, C., Serwatowski, P., Gatzemeier, U., Digumarti, R., Zukin, M., et al. (2008). Phase III study comparing cisplatin plus gemcitabine with cisplatin plus pemetrexed in chemotherapy-naive patients with advanced-stage non-small-cell lung cancer. J. Clin. Oncol. *26*, 3543–3551.

Schiller, J.H., Harrington, D., Belani, C.P., Langer, C., Sandler, A., Krook, J., Zhu, J., and Johnson, D.H.; Eastern Cooperative Oncology Group (2002). Comparison of four chemotherapy regimens for advanced non-small-cell lung cancer. N. Engl. J. Med. *346*, 92–98.

Sharma, S.V., Lee, D.Y., Li, B., Quinlan, M.P., Takahashi, F., Maheswaran, S., McDermott, U., Azizian, N., Zou, L., Fischbach, M.A., et al. (2010). A chromatin-mediated reversible drug-tolerant state in cancer cell subpopulations. Cell *141*, 69–80.

Subramanian, A., Tamayo, P., Mootha, V.K., Mukherjee, S., Ebert, B.L., Gillette, M.A., Paulovich, A., Pomeroy, S.L., Golub, T.R., Lander, E.S., and Mesirov, J.P. (2005). Gene set enrichment analysis: a knowledge-based approach for interpreting genome-wide expression profiles. Proc. Natl. Acad. Sci. USA *102*, 15545–15550.

Szakács, G., Paterson, J.K., Ludwig, J.A., Booth-Genthe, C., and Gottesman, M.M. (2006). Targeting multidrug resistance in cancer. Nat. Rev. Drug Discov. *5*, 219–234.

Szenker, E., Ray-Gallet, D., and Almouzni, G. (2011). The double face of the histone variant H3.3. Cell Res. *21*, 421–434.

Vinogradova, M., Gehling, V.S., Gustafson, A., Arora, S., Tindell, C.A., Wilson, C., Williamson, K.E., Guler, G.D., Gangurde, P., Manieri, W., et al. (2016). An inhibitor of KDM5 demethylases reduces survival of drug-tolerant cancer cells. Nat. Chem. Biol. *12*, 531–538.

Wang, L., Chang, J., Varghese, D., Dellinger, M., Kumar, S., Best, A.M., Ruiz, J., Bruick, R., Peña-Llopis, S., Xu, J., et al. (2013). A small molecule modulates Jumonji histone demethylase activity and selectively inhibits cancer growth. Nat. Commun. *4*, 2035.

Wilson, C., Ye, X., Pham, T., Lin, E., Chan, S., McNamara, E., Neve, R.M., Belmont, L., Koeppen, H., Yauch, R.L., et al. (2014). AXL inhibition sensitizes mesenchymal cancer cells to antimitotic drugs. Cancer Res. *74*, 5878–5890.